

Precise measurement of the D^0 and D^+ lifetimes at Belle II

F. Abudinén,³¹ I. Adachi,^{21,18} K. Adamczyk,⁶⁶ L. Aggarwal,⁷³ H. Ahmed,⁷⁶ H. Aihara,¹¹² N. Akopov,² A. Aloisio,^{88,25} N. Anh Ky,^{40,13} D. M. Asner,³ H. Atmacan,⁹⁹ V. Aushev,⁸¹ V. Babu,¹¹ S. Bacher,⁶⁶ H. Bae,¹¹² S. Baehr,⁴⁶ S. Bahinipati,³³ P. Bambade,⁹⁵ Sw. Banerjee,¹⁰³ S. Bansal,⁷³ M. Barrett,²¹ J. Baudot,⁹⁶ M. Bauer,⁴⁶ A. Baur,¹¹ J. Becker,⁴⁶ P. K. Behera,³⁵ J. V. Bennett,¹⁰⁶ E. Bernieri,²⁹ F. U. Bernlochner,⁹⁷ M. Bertemes,³⁸ E. Bertholet,⁸⁴ M. Bessner,¹⁰¹ S. Bettarini,^{91,28} V. Bhardwaj,³² F. Bianchi,^{93,30} T. Bilka,⁷ S. Bilokin,⁵⁴ D. Biswas,¹⁰³ A. Bobrov,^{4,68} D. Bodrov,^{64,52} A. Bolz,¹¹ A. Bozek,⁶⁶ M. Bračko,^{104,80} P. Branchini,²⁹ N. Braun,⁴⁶ R. A. Briere,⁵ T. E. Browder,¹⁰¹ A. Budano,²⁹ S. Bussino,^{92,29} M. Campajola,^{88,25} L. Cao,¹¹ G. Casarosa,^{91,28} C. Cecchi,^{90,27} D. Červenkov,⁷ M.-C. Chang,¹⁵ P. Chang,⁶⁵ R. Cheaib,¹¹ V. Chekelian,⁵⁷ C. Chen,⁴² Y.-T. Chen,⁶⁵ B. G. Cheon,²⁰ K. Chilikin,⁵² K. Chirapatpimol,⁸ H.-E. Cho,²⁰ K. Cho,⁴⁸ S.-J. Cho,¹¹⁸ S.-K. Choi,¹⁹ S. Choudhury,³⁴ D. Cinabro,¹¹⁶ L. Corona,^{91,28} L. M. Cremaldi,¹⁰⁶ S. Cunliffe,¹¹ T. Czank,¹¹³ F. Dattola,¹¹ E. De La Cruz-Burelo,⁶ G. de Marino,⁹⁵ G. De Nardo,^{88,25} G. De Pietro,²⁹ R. de Sangro,²⁴ M. Destefanis,^{93,30} S. Dey,⁸⁴ A. De Yta-Hernandez,⁶ A. Di Canto,³ F. Di Capua,^{88,25} J. Dingfelder,⁹⁷ Z. Doležal,⁷ I. Domínguez Jiménez,⁸⁷ T. V. Dong,¹³ M. Dorigo,³¹ K. Dort,⁴⁵ D. Dossett,¹⁰⁵ S. Dubey,¹⁰¹ S. Duell,⁹⁷ G. Dujany,⁹⁶ P. Ecker,⁴⁶ D. Epifanov,^{4,68} T. Ferber,¹¹ D. Ferlewicz,¹⁰⁵ G. Finocchiaro,²⁴ K. Flood,¹⁰¹ A. Fodor,⁵⁸ F. Forti,^{91,28} B. G. Fulsom,⁷² A. Gabrielli,^{94,31} N. Gabyshev,^{4,68} A. Gaz,^{89,26} A. Gellrich,¹¹ G. Giakoustidis,⁹⁷ R. Giordano,^{88,25} A. Giri,³⁴ A. Glazov,¹¹ B. Gobbo,³¹ R. Godang,¹¹⁰ P. Goldenzweig,⁴⁶ B. Golob,^{102,80} W. Gradl,⁴⁴ E. Graziani,²⁹ D. Greenwald,⁸³ T. Gu,¹⁰⁸ Y. Guan,⁹⁹ K. Gudkova,^{4,68} J. Guillems,¹⁰⁶ C. Hadjivasilou,⁷² S. Halder,⁸² K. Hara,^{21,18} T. Hara,^{21,18} O. Hartbrich,¹⁰¹ K. Hayasaka,⁶⁷ H. Hayashii,⁶³ S. Hazra,⁸² C. Hearty,^{98,39} I. Heredia de la Cruz,^{6,10} M. Hernández Villanueva,¹¹ A. Hershenhorn,⁹⁸ T. Higuchi,¹¹³ E. C. Hill,⁹⁸ H. Hirata,⁶⁰ M. Hoek,⁴⁴ M. Hohmann,¹⁰⁵ C.-L. Hsu,¹¹¹ T. Humair,⁵⁷ T. Iijima,^{60,62} K. Inami,⁶⁰ G. Inguglia,³⁸ A. Ishikawa,^{21,18} R. Itoh,^{21,18} M. Iwasaki,⁷⁰ Y. Iwasaki,²¹ W. W. Jacobs,³⁶ D. E. Jaffe,³ E.-J. Jang,¹⁹ S. Jia,¹⁶ Y. Jin,³¹ H. Junkerkalefeld,⁹⁷ H. Kakuno,⁸⁶ A. B. Kaliyar,⁸² J. Kandra,⁷ K. H. Kang,⁵¹ R. Karl,¹¹ G. Karyan,² Y. Kato,^{60,62} T. Kawasaki,⁴⁷ C. Kiesling,⁵⁷ C.-H. Kim,²⁰ D. Y. Kim,⁷⁹ Y.-K. Kim,¹¹⁸ Y. Kim,⁴⁹ T. D. Kimmel,¹¹⁵ K. Kinoshita,⁹⁹ P. Kodyš,⁷ T. Koga,²¹ S. Kohani,¹⁰¹ T. Konno,⁴⁷ S. Korpar,^{104,80} E. Kovalenko,^{4,68} R. Kowalewski,¹¹⁴ T. M. G. Kraetzschmar,⁵⁷ F. Krinner,⁵⁷ P. Križan,^{102,80} P. Krokovny,^{4,68} T. Kuhr,⁵⁴ J. Kumar,⁵ M. Kumar,⁵⁶ R. Kumar,⁷⁴ K. Kumara,¹¹⁶ S. Kurz,¹¹ A. Kuzmin,^{4,68} Y.-J. Kwon,¹¹⁸ S. Lacaprara,²⁶ K. Lalwani,⁵⁶ T. Lam,¹¹⁵ L. Lancieri,³¹ J. S. Lange,⁴⁵ M. Laurenza,^{92,29} K. Lautenbach,¹ F. R. Le Diberder,⁹⁵ S. C. Lee,⁵¹ P. Leitl,⁵⁷ D. Levit,⁸³ C. Li,⁵³ L. K. Li,⁹⁹ J. Libby,³⁵ K. Lieret,⁵⁴ Z. Liptak,²³ Q. Y. Liu,¹¹ D. Liventsev,^{116,21} S. Longo,¹¹ T. Lueck,⁵⁴ C. Lyu,⁹⁷ R. Manfredi,^{94,31} E. Manoni,²⁷ C. Marinus,⁴¹ A. Martini,¹¹ T. Matsuda,¹⁰⁷ K. Matsuoka,²¹ D. Matvienko,^{4,52,68} J. A. McKenna,⁹⁸ F. Meier,¹² M. Merola,^{88,25} F. Metzner,⁴⁶ C. Miller,¹¹⁴ K. Miyabayashi,⁶³ R. Mizuk,^{52,64} G. B. Mohanty,⁸² N. Molina-Gonzalez,⁶ H. Moon,⁴⁹ H.-G. Moser,⁹⁷ M. Mrvar,³⁸ C. Murphy,¹¹³ R. Mussa,³⁰ I. Nakamura,^{21,18} K. R. Nakamura,^{21,18} M. Nakao,^{21,18} H. Nakazawa,⁶⁵ Z. Natkaniec,⁶⁶ A. Natochii,¹⁰¹ G. Nazaryan,² C. Niebuhr,¹¹ M. Niiyama,⁵⁰ N. K. Nisar,³ S. Nishida,^{21,18} K. Nishimura,¹⁰¹ S. Ogawa,⁸⁵ Y. Onishchuk,⁸¹ H. Ono,⁶⁷ Y. Onuki,¹¹² P. Oskin,⁵² E. R. Oxford,⁵ H. Ozaki,^{21,18} P. Pakhlov,^{52,59} A. Paladino,^{91,28} T. Pang,¹⁰⁸ A. Panta,¹⁰⁶ E. Paoloni,^{91,28} S. Pardi,²⁵ H. Park,⁵¹ S.-H. Park,²¹ B. Paschen,⁹⁷ A. Passeri,²⁹ A. Pathak,¹⁰³ S. Patra,³² S. Paul,⁸³ T. K. Pedlar,⁵⁵ I. Peruzzi,²⁴ R. Peschke,¹⁰¹ R. Pestotnik,⁸⁰ F. Pham,¹⁰⁵ M. Piccolo,²⁴ L. E. Pilonen,¹¹⁵ G. Pinna Angioni,^{93,30} P. L. M. Podesta-Lerma,⁸⁷ T. Podobnik,⁸⁰ S. Pokharel,¹⁰⁶ G. Polat,¹ V. Popov,⁶⁴ C. Praz,¹¹ S. Prell,⁴² E. Prencipe,⁴⁵ M. T. Prim,⁹⁷ M. V. Purohit,⁶⁹ H. Purwar,¹⁰¹ N. Rad,¹¹ P. Rados,³⁸ S. Raiz,^{94,31} S. Reiter,⁴⁵ M. Remnev,^{4,68} I. Ripp-Baudot,⁹⁶ G. Rizzo,^{91,28} L. B. Rizzuto,⁸⁰ S. H. Robertson,^{58,39} J. M. Roney,^{114,39} A. Rostomyan,¹¹ N. Rout,³⁵ M. Rozanska,⁶⁶ D. Sahoo,⁴² D. A. Sanders,¹⁰⁶ S. Sandilya,³⁴ A. Sangal,⁹⁹ L. Santelj,^{102,80} Y. Sato,²¹ V. Savinov,¹⁰⁸ B. Scavino,⁴⁴ J. Schueler,¹⁰¹ C. Schwanda,³⁸ A. J. Schwartz,⁹⁹ Y. Seino,⁶⁷ A. Selce,^{29,14} K. Senyo,¹¹⁷ J. Serrano,¹ C. Sfienti,⁴⁴ J.-G. Shiu,⁶⁵ B. Shwartz,^{4,68} A. Sibidanov,¹⁰¹ F. Simon,⁵⁷ R. J. Sobie,^{114,39} A. Soffer,⁸⁴ A. Sokolov,³⁷ E. Solovieva,⁵² S. Spataro,^{93,30} B. Spruck,⁴⁴ M. Starič,⁸⁰ S. Stefkova,¹¹ Z. S. Stottler,¹¹⁵ R. Stroili,^{89,26} J. Strube,⁷² M. Sumihama,^{17,71} W. Sutcliffe,⁹⁷ S. Y. Suzuki,^{21,18} H. Svidras,¹¹ M. Tabata,⁹ M. Takizawa,^{75,22,77} U. Tamponi,³⁰ S. Tanaka,^{21,18} K. Tanida,⁴³ H. Tanigawa,¹¹² N. Taniguchi,²¹ F. Tenchini,^{91,28} R. Tiwary,⁸² D. Tonelli,³¹ E. Torassa,²⁶ N. Toutounji,¹¹¹ K. Trabelsi,⁹⁵ T. Tsuboyama,^{21,18} I. Ueda,^{21,18} S. Uehara,^{21,18} Y. Uematsu,¹¹² T. Uglov,^{52,64} K. Unger,⁴⁶ Y. Unno,²⁰ K. Uno,⁶⁷ S. Uno,^{21,18} P. Urquijo,¹⁰⁵ Y. Ushiroda,^{21,18,112} Y. V. Usov,^{4,68} S. E. Vahsen,¹⁰¹ R. van Tonder,⁹⁷ G. S. Varner,¹⁰¹ A. Vinokurova,^{4,68} L. Vitale,^{94,31} A. Vossen,¹² E. Waheed,²¹ H. M. Wakeling,⁵⁸ E. Wang,¹⁰⁸ M.-Z. Wang,⁶⁵ X. L. Wang,¹⁶

A. Warburton,⁵⁸ M. Watanabe,⁶⁷ M. Welsch,⁹⁷ C. Wessel,⁹⁷ J. Wiechczynski,⁶⁶ E. Won,⁴⁹ X. P. Xu,⁷⁸
 B. D. Yabsley,¹¹¹ S. Yamada,²¹ W. Yan,¹⁰⁹ S. B. Yang,⁴⁹ H. Ye,¹¹ J. Yelton,¹⁰⁰ J. H. Yin,⁴⁹ K. Yoshihara,⁶⁰
 Y. Yusa,⁶⁷ L. Zani,¹ V. Zhilich,^{4, 68} Q. D. Zhou,^{60, 61, 62} X. Y. Zhou,⁵³ V. I. Zhukova,⁵² and R. Žlebčík⁷

(Belle II Collaboration)

¹*Aix Marseille Université, CNRS/IN2P3, CPPM, 13288 Marseille, France*

²*Alikhanyan National Science Laboratory, Yerevan 0036, Armenia*

³*Brookhaven National Laboratory, Upton, New York 11973, U.S.A.*

⁴*Budker Institute of Nuclear Physics SB RAS, Novosibirsk 630090, Russian Federation*

⁵*Carnegie Mellon University, Pittsburgh, Pennsylvania 15213, U.S.A.*

⁶*Centro de Investigacion y de Estudios Avanzados del Instituto Politécnico Nacional, Mexico City 07360, Mexico*

⁷*Faculty of Mathematics and Physics, Charles University, 121 16 Prague, Czech Republic*

⁸*Chiang Mai University, Chiang Mai 50202, Thailand*

⁹*Chiba University, Chiba 263-8522, Japan*

¹⁰*Consejo Nacional de Ciencia y Tecnología, Mexico City 03940, Mexico*

¹¹*Deutsches Elektronen-Synchrotron, 22607 Hamburg, Germany*

¹²*Duke University, Durham, North Carolina 27708, U.S.A.*

¹³*Institute of Theoretical and Applied Research (ITAR), Duy Tan University, Hanoi 100000, Vietnam*

¹⁴*ENEA Casaccia, I-00123 Roma, Italy*

¹⁵*Department of Physics, Fu Jen Catholic University, Taipei 24205, Taiwan*

¹⁶*Key Laboratory of Nuclear Physics and Ion-beam Application (MOE) and
 Institute of Modern Physics, Fudan University, Shanghai 200443, China*

¹⁷*Gifu University, Gifu 501-1193, Japan*

¹⁸*The Graduate University for Advanced Studies (SOKENDAI), Hayama 240-0193, Japan*

¹⁹*Gyeongsang National University, Jinju 52828, South Korea*

²⁰*Department of Physics and Institute of Natural Sciences, Hanyang University, Seoul 04763, South Korea*

²¹*High Energy Accelerator Research Organization (KEK), Tsukuba 305-0801, Japan*

²²*J-PARC Branch, KEK Theory Center, High Energy Accelerator Research Organization (KEK), Tsukuba 305-0801, Japan*

²³*Hiroshima University, Higashi-Hiroshima, Hiroshima 739-8530, Japan*

²⁴*INFN Laboratori Nazionali di Frascati, I-00044 Frascati, Italy*

²⁵*INFN Sezione di Napoli, I-80126 Napoli, Italy*

²⁶*INFN Sezione di Padova, I-35131 Padova, Italy*

²⁷*INFN Sezione di Perugia, I-06123 Perugia, Italy*

²⁸*INFN Sezione di Pisa, I-56127 Pisa, Italy*

²⁹*INFN Sezione di Roma Tre, I-00146 Roma, Italy*

³⁰*INFN Sezione di Torino, I-10125 Torino, Italy*

³¹*INFN Sezione di Trieste, I-34127 Trieste, Italy*

³²*Indian Institute of Science Education and Research Mohali, SAS Nagar, 140306, India*

³³*Indian Institute of Technology Bhubaneswar, Satya Nagar 751007, India*

³⁴*Indian Institute of Technology Hyderabad, Telangana 502285, India*

³⁵*Indian Institute of Technology Madras, Chennai 600036, India*

³⁶*Indiana University, Bloomington, Indiana 47408, U.S.A.*

³⁷*Institute for High Energy Physics, Protvino 142281, Russian Federation*

³⁸*Institute of High Energy Physics, Vienna 1050, Austria*

³⁹*Institute of Particle Physics (Canada), Victoria, British Columbia V8W 2Y2, Canada*

⁴⁰*Institute of Physics, Vietnam Academy of Science and Technology (VAST), Hanoi, Vietnam*

⁴¹*Instituto de Física Corpuscular, Paterna 46980, Spain*

⁴²*Iowa State University, Ames, Iowa 50011, U.S.A.*

⁴³*Advanced Science Research Center, Japan Atomic Energy Agency, Naka 319-1195, Japan*

⁴⁴*Institut für Kernphysik, Johannes Gutenberg-Universität Mainz, D-55099 Mainz, Germany*

⁴⁵*Justus-Liebig-Universität Gießen, 35392 Gießen, Germany*

⁴⁶*Institut für Experimentelle Teilchenphysik, Karlsruher Institut für Technologie, 76131 Karlsruhe, Germany*

⁴⁷*Kitasato University, Sagamihara 252-0373, Japan*

⁴⁸*Korea Institute of Science and Technology Information, Daejeon 34141, South Korea*

⁴⁹*Korea University, Seoul 02841, South Korea*

⁵⁰*Kyoto Sangyo University, Kyoto 603-8555, Japan*

⁵¹*Kyungpook National University, Daegu 41566, South Korea*

⁵²*P.N. Lebedev Physical Institute of the Russian Academy of Sciences, Moscow 119991, Russian Federation*

⁵³*Liaoning Normal University, Dalian 116029, China*

⁵⁴*Ludwig Maximilians University, 80539 Munich, Germany*

⁵⁵*Luther College, Decorah, Iowa 52101, U.S.A.*

⁵⁶*Malaviya National Institute of Technology Jaipur, Jaipur 302017, India*

⁵⁷*Max-Planck-Institut für Physik, 80805 München, Germany*

- ⁵⁸ McGill University, Montréal, Québec, H3A 2T8, Canada
- ⁵⁹ Moscow Physical Engineering Institute, Moscow 115409, Russian Federation
- ⁶⁰ Graduate School of Science, Nagoya University, Nagoya 464-8602, Japan
- ⁶¹ Institute for Advanced Research, Nagoya University, Nagoya 464-8602, Japan
- ⁶² Kobayashi-Maskawa Institute, Nagoya University, Nagoya 464-8602, Japan
- ⁶³ Nara Women's University, Nara 630-8506, Japan
- ⁶⁴ National Research University Higher School of Economics, Moscow 101000, Russian Federation
- ⁶⁵ Department of Physics, National Taiwan University, Taipei 10617, Taiwan
- ⁶⁶ H. Niewodniczanski Institute of Nuclear Physics, Krakow 31-342, Poland
- ⁶⁷ Niigata University, Niigata 950-2181, Japan
- ⁶⁸ Novosibirsk State University, Novosibirsk 630090, Russian Federation
- ⁶⁹ Okinawa Institute of Science and Technology, Okinawa 904-0495, Japan
- ⁷⁰ Osaka City University, Osaka 558-8585, Japan
- ⁷¹ Research Center for Nuclear Physics, Osaka University, Osaka 567-0047, Japan
- ⁷² Pacific Northwest National Laboratory, Richland, Washington 99352, U.S.A.
- ⁷³ Panjab University, Chandigarh 160014, India
- ⁷⁴ Punjab Agricultural University, Ludhiana 141004, India
- ⁷⁵ Meson Science Laboratory, Cluster for Pioneering Research, RIKEN, Saitama 351-0198, Japan
- ⁷⁶ St. Francis Xavier University, Antigonish, Nova Scotia, B2G 2W5, Canada
- ⁷⁷ Showa Pharmaceutical University, Tokyo 194-8543, Japan
- ⁷⁸ Soochow University, Suzhou 215006, China
- ⁷⁹ Soongsil University, Seoul 06978, South Korea
- ⁸⁰ J. Stefan Institute, 1000 Ljubljana, Slovenia
- ⁸¹ Taras Shevchenko National Univ. of Kiev, Kiev, Ukraine
- ⁸² Tata Institute of Fundamental Research, Mumbai 400005, India
- ⁸³ Department of Physics, Technische Universität München, 85748 Garching, Germany
- ⁸⁴ Tel Aviv University, School of Physics and Astronomy, Tel Aviv, 69978, Israel
- ⁸⁵ Toho University, Funabashi 274-8510, Japan
- ⁸⁶ Tokyo Metropolitan University, Tokyo 192-0397, Japan
- ⁸⁷ Universidad Autonoma de Sinaloa, Sinaloa 80000, Mexico
- ⁸⁸ Dipartimento di Scienze Fisiche, Università di Napoli Federico II, I-80126 Napoli, Italy
- ⁸⁹ Dipartimento di Fisica e Astronomia, Università di Padova, I-35131 Padova, Italy
- ⁹⁰ Dipartimento di Fisica, Università di Perugia, I-06123 Perugia, Italy
- ⁹¹ Dipartimento di Fisica, Università di Pisa, I-56127 Pisa, Italy
- ⁹² Dipartimento di Matematica e Fisica, Università di Roma Tre, I-00146 Roma, Italy
- ⁹³ Dipartimento di Fisica, Università di Torino, I-10125 Torino, Italy
- ⁹⁴ Dipartimento di Fisica, Università di Trieste, I-34127 Trieste, Italy
- ⁹⁵ Université Paris-Saclay, CNRS/IN2P3, IJCLab, 91405 Orsay, France
- ⁹⁶ Université de Strasbourg, CNRS, IPHC, UMR 7178, 67037 Strasbourg, France
- ⁹⁷ University of Bonn, 53115 Bonn, Germany
- ⁹⁸ University of British Columbia, Vancouver, British Columbia, V6T 1Z1, Canada
- ⁹⁹ University of Cincinnati, Cincinnati, Ohio 45221, U.S.A.
- ¹⁰⁰ University of Florida, Gainesville, Florida 32611, U.S.A.
- ¹⁰¹ University of Hawaii, Honolulu, Hawaii 96822, U.S.A.
- ¹⁰² Faculty of Mathematics and Physics, University of Ljubljana, 1000 Ljubljana, Slovenia
- ¹⁰³ University of Louisville, Louisville, Kentucky 40292, U.S.A.
- ¹⁰⁴ Faculty of Chemistry and Chemical Engineering, University of Maribor, 2000 Maribor, Slovenia
- ¹⁰⁵ School of Physics, University of Melbourne, Victoria 3010, Australia
- ¹⁰⁶ University of Mississippi, University, Mississippi 38677, U.S.A.
- ¹⁰⁷ University of Miyazaki, Miyazaki 889-2192, Japan
- ¹⁰⁸ University of Pittsburgh, Pittsburgh, Pennsylvania 15260, U.S.A.
- ¹⁰⁹ University of Science and Technology of China, Hefei 230026, China
- ¹¹⁰ University of South Alabama, Mobile, Alabama 36688, U.S.A.
- ¹¹¹ School of Physics, University of Sydney, New South Wales 2006, Australia
- ¹¹² Department of Physics, University of Tokyo, Tokyo 113-0033, Japan
- ¹¹³ Kavli Institute for the Physics and Mathematics of the Universe (WPI), University of Tokyo, Kashiwa 277-8583, Japan
- ¹¹⁴ University of Victoria, Victoria, British Columbia, V8W 3P6, Canada
- ¹¹⁵ Virginia Polytechnic Institute and State University, Blacksburg, Virginia 24061, U.S.A.
- ¹¹⁶ Wayne State University, Detroit, Michigan 48202, U.S.A.
- ¹¹⁷ Yamagata University, Yamagata 990-8560, Japan
- ¹¹⁸ Yonsei University, Seoul 03722, South Korea

We report a measurement of the D^0 and D^+ lifetimes using $D^0 \rightarrow K^-\pi^+$ and $D^+ \rightarrow K^-\pi^+\pi^+$ decays reconstructed in $e^+e^- \rightarrow c\bar{c}$ data recorded by the Belle II experiment at the SuperKEKB

asymmetric-energy e^+e^- collider. The data correspond to an integrated luminosity of 72 fb^{-1} . The results, $\tau(D^0) = 410.5 \pm 1.1 \text{ (stat)} \pm 0.8 \text{ (syst)} \text{ fs}$ and $\tau(D^+) = 1030.4 \pm 4.7 \text{ (stat)} \pm 3.1 \text{ (syst)} \text{ fs}$, are the most precise to date and are consistent with previous determinations.

Accurate predictions of lifetimes of weakly decaying charmed and bottom hadrons are challenging because they involve strong-interaction theory at low energy. Predictions must resort to effective models, such as the heavy-quark expansion [1–6], which also underpin strong-interaction calculations required for the determination of fundamental standard-model parameters from hadron-decay measurements (*e.g.*, to extract the strength of quark-mixing couplings from decay widths). Precise lifetime measurements provide excellent tests of such effective models. Lifetimes are also important inputs for a wide variety of studies because they are needed to compare measured decay branching fractions to predictions for partial decay-widths.

Weakly decaying charmed hadrons have lifetimes ranging from about 0.1 to 1 ps [7]. The world averages of the D^0 and D^+ lifetimes, $410.1 \pm 1.5 \text{ fs}$ and $1040 \pm 7 \text{ fs}$, are almost exclusively determined from systematically-limited per-mille-precision measurements made by FOCUS two decades ago [7, 8]. Recently, LHCb precisely measured the lifetimes of the D_s^+ meson and charmed baryons relative to that of the D^+ meson [9–12]. Such relative measurements minimize systematic uncertainties due to decay-time-biasing event-selection criteria that are particularly severe at hadron colliders. By contrast, experiments at e^+e^- colliders, owing to the reconstruction of large charmed hadron yields without decay-time-biasing selections, have a great potential for absolute lifetime measurements. With the first layer of its vertex detector only 1.4 cm away from the interaction region, the Belle II experiment at the SuperKEKB asymmetric-energy e^+e^- collider [13, 14] obtains a decay-time resolution two times better than the Belle and BABAR experiments [15], enabling high precision for the measurement of charmed lifetimes with early data. To limit systematic uncertainties this potential must be complemented with an accurate vertex-detector alignment, a precise calibration of final-state particle momenta, and powerful background discrimination.

In this Letter, we report high-precision measurements of the D^0 and D^+ lifetimes using $D^{*+} \rightarrow D^0(\rightarrow K^-\pi^+)\pi^+$ and $D^{*+} \rightarrow D^+(\rightarrow K^-\pi^+\pi^+)\pi^0$ decays reconstructed in the data collected by Belle II during 2019 and the first half of 2020, corresponding to an integrated luminosity of 72 fb^{-1} . (Charge-conjugate decays are implied throughout.) At Belle II, D^{*+} mesons from $e^+e^- \rightarrow c\bar{c}$ events are produced with boosts that displace the D^0 - and D^+ -meson decay points from those of production by approximately $200 \mu\text{m}$ and $500 \mu\text{m}$ on average, respectively. The decay time is measured from this displacement, \vec{L} , projected onto the direction of the

momentum, \vec{p} , as $t = m_D \vec{L} \cdot \vec{p} / (|\vec{p}|^2 c)$, where m_D is the known mass of the relevant D meson [7]. The decay-time uncertainty, σ_t , is calculated by propagating the uncertainties in \vec{L} and \vec{p} , including their correlations. The lifetimes are measured using a fit to the (t, σ_t) distributions of the reconstructed decay candidates. The sample selection and fit strategy have been optimized and validated using simulation; however, no input from simulation is used in the fit to data. To avoid bias, we inspected the lifetimes measured with the full data sample only after the entire analysis procedure was finalized and all uncertainties were determined. However, we examined the results from the subset of data collected during 2019 (approximately 13% of the total) before the analysis was complete.

The Belle II detector [13] consists of several subsystems arranged in a cylindrical structure around the beam pipe. The tracking system consists of a two-layer silicon-pixel detector (PXD), surrounded by a four-layer double-sided silicon-strip detector (SVD) and a central drift chamber (CDC). Only two out of 12 ladders were installed in the second layer of the PXD for this data sample. The combined PXD and SVD system provides average decay-time resolutions of about 70 fs and 60 fs, respectively, for the D^0 and D^+ decays considered here. A time-of-propagation counter and an aerogel ring-imaging Cherenkov counter that cover the barrel and forward end-cap regions of the detector, respectively, are essential for charged-particle identification. The electromagnetic calorimeter fills the remaining volume inside a 1.5 T superconducting solenoid and serves to reconstruct photons and electrons. A dedicated system to identify K_L^0 mesons and muons is installed in the outermost part of the detector. The z axis of the laboratory frame is defined as the central axis of the solenoid, with its positive direction determined by the direction of the electron beam.

The simulation uses KKMC [16] to generate quark-antiquark pairs from e^+e^- collisions, PYTHIA8 [17] for hadronization, EVTGEN [18] for the decay of the generated hadrons, and GEANT4 [19] for the detector response.

The reconstruction [20] and selection of the signal candidates avoid any requirement that could bias the decay time or introduce a variation of the efficiency as a function of decay time, as checked in simulation. Events are first selected by vetoing events consistent with Bhabha scattering and by requiring at least three tracks with loose upper bounds on their impact parameters and with transverse momenta greater than $200 \text{ MeV}/c$.

Candidate $D^0 \rightarrow K^-\pi^+$ decays are formed using pairs of oppositely charged tracks. Each track must have a hit in the first layer of the PXD, at least one hit in the SVD,

at least 20 hits in the CDC, and be identified as a pion or kaon. Low-momentum pion candidates are tracks consistent with originating from the interaction region that have at least one hit in the SVD and at least one hit in the CDC. They are combined with D^0 candidates to form $D^{*+} \rightarrow D^0\pi^+$ decays. A global decay-chain vertex fit [21] constrains the tracks according to the decay topology and constrains the D^{*+} candidate to originate from the measured position of the e^+e^- interaction region (IR). Only candidates with fit χ^2 probabilities larger than 0.01 are retained for further analysis. The IR has typical dimensions of 250 μm along z and of 10 μm and 0.3 μm in the transverse plane. Its position and size vary over data-taking and are regularly measured using $e^+e^- \rightarrow \mu^+\mu^-$ events. The mass of the D^0 candidate, $m(K^-\pi^+)$, must be in the range [1.75, 2.00] GeV/c^2 . The difference between the D^{*+} - and D^0 -candidate masses, Δm , must satisfy $144.94 < \Delta m < 145.90 \text{ MeV}/c^2$ (± 3 times the Δm resolution around the peak of the signal distribution). Since the D^0 is assumed to originate from the IR, charmed mesons originating from displaced decays of bottom mesons would bias the lifetime measurement. They are suppressed to a negligible rate by requiring that the momentum of the D^{*+} in the e^+e^- center-of-mass system exceeds 2.5 GeV/c . After requiring $1.851 < m(K^-\pi^+) < 1.878 \text{ GeV}/c^2$ (signal region), multiple D^{*+} candidates occur in a few per mille of the selected events. In such events, one randomly selected candidate is retained for subsequent analysis.

The signal region contains approximately 171×10^3 candidates with a signal purity of about 99.8%, as determined from a binned least-squares fit to the $m(K^-\pi^+)$ distribution (Fig. 1). In the fit, the $D^0 \rightarrow K^-\pi^+$ signal is modeled with the sum of two Gaussian distributions and a Crystal-Ball function [22]; misidentified decays of $D^0 \rightarrow \pi^+\pi^-$ and $D^0 \rightarrow K^+K^-$, each modeled with a Johnson's S_U distribution [23] with parameters determined from simulation, do not enter the signal region; the remaining background, modeled with an exponential distribution, is dominated by candidates formed by random combinations of particles.

The selection of the $D^{*+} \rightarrow D^+(\rightarrow K^-\pi^+\pi^+)\pi^0$ candidates follows similar criteria to those for the D^0 mode, but with more stringent requirements to suppress a larger background contamination. Candidate kaons and pions are required to have a hit in the first layer of the PXD, at least one hit in the SVD, and at least 30 hits in the CDC. They are combined to form $D^+ \rightarrow K^-\pi^+\pi^+$ candidates. To suppress backgrounds from misreconstructed charmed-hadron decays, such as four-body hadronic or semileptonic decays, the lower-momentum pion must have momentum exceeding 350 MeV/c and the higher-momentum pion must not be identified as a lepton. Candidate $\pi^0 \rightarrow \gamma\gamma$ decays are reconstructed using photon candidates from calorimetric energy clusters that are not associated with a track. Each photon energy

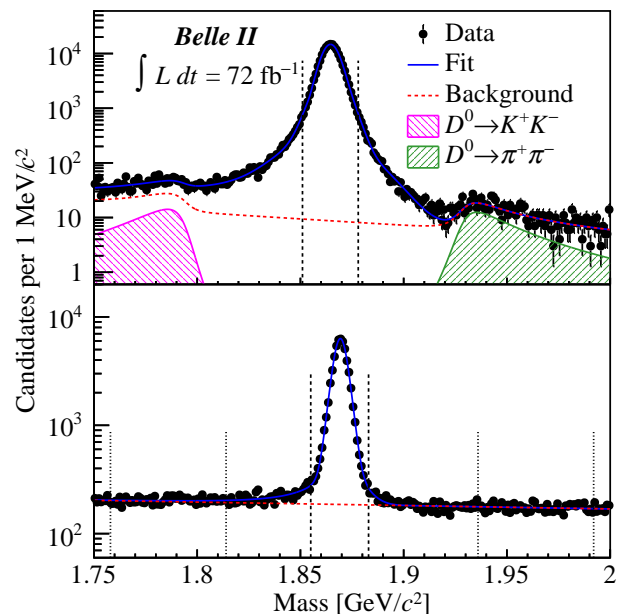


Figure 1: Mass distributions of (top) $D^0 \rightarrow K^-\pi^+$ and (bottom) $D^+ \rightarrow K^-\pi^+\pi^+$ candidates with fit projections overlaid. The vertical dashed and (for the bottom plot) dotted lines indicate the signal regions and the sideband, respectively.

must be larger than 80, 30, or 60 MeV if detected in the forward, central, or backward region, respectively, of the calorimeter. Neutral-pion candidates with masses in the range [120, 145] MeV/c^2 and momenta larger than 150 MeV/c are combined with D^+ candidates to form $D^{*+} \rightarrow D^+\pi^0$ decays. The D^{*+} decay chain is fit using IR and π^0 -mass constraints. Only candidates with fit χ^2 probabilities larger than 0.01 are retained. The mass of the D^+ candidate, $m(K^-\pi^+\pi^+)$, must be in the range [1.75, 2.00] GeV/c^2 and the difference between the D^{*+} and D^+ masses in the range [138, 143] MeV/c^2 (± 3 times the Δm resolution around the peak of the signal distribution). The momentum of the D^{*+} in the e^+e^- center-of-mass system must exceed 2.6 GeV/c to suppress D^{*+} candidates from bottom mesons. This requirement is tighter than that used for D^0 candidates because of the less-precise π^0 -momentum resolution.

The signal region in $m(K^-\pi^+\pi^+)$ is defined as [1.855, 1.883] GeV/c^2 (Fig. 1). It contains approximately 59×10^3 candidates after randomly selecting one D^{*+} candidate for the percent-level fraction of events where more than one is found. A binned least-squares fit to the $m(K^-\pi^+\pi^+)$ distribution identifies about 9% of candidates in the signal region as background. Simulation shows that such background is composed of misreconstructed charmed decays and random track combinations. In the fit, the $D^+ \rightarrow K^-\pi^+\pi^+$ signal is modeled with the sum of two Gaussian distributions and a Crystal-Ball function; the background is modeled with an exponential distribution.

The lifetimes are determined using unbinned maximum-likelihood fits to the (t, σ_t) distributions of the candidates populating the signal regions. Each signal probability-density function (PDF) is the convolution of an exponential distribution in t with a resolution function that depends on σ_t , multiplied by the PDF of σ_t . In the D^+ case, simulation shows that a Gaussian distribution is sufficient to model the resolution function. The mean of the resolution function is allowed to float in the fit to account for a possible bias in the determination of the decay time; the width is the per-candidate σ_t scaled by a free parameter s to account for a possible misestimation of the decay-time uncertainty. In the D^0 case, an additional Gaussian distribution is needed to describe the 3% of candidates with poorer resolution. This second component shares its mean with the principal component but has its own free scaling parameter for the broader width.

In the D^0 case, the signal region contains a per-mille-level fraction of background candidates. Sensitivity to the background contamination and its effects on the decay-time distribution is very limited. For the sake of simplicity, the background is neglected in the fit and a systematic uncertainty is later assigned. In the D^+ case, the signal region contains a non-negligible amount of background, which is accounted for in the fit. The background is modeled using data with $m(K^-\pi^+\pi^+)$ in the *sideband* $[1.758, 1.814] \cup [1.936, 1.992]$ GeV/c^2 (Fig. 1), which is assumed to contain exclusively background candidates and be representative of the background in the signal region, as verified in simulation. The background PDF consists of a zero-lifetime component and two exponential components, all convolved with a Gaussian resolution function having a free mean and a width corresponding to σ_t . To better constrain the background parameters, a simultaneous fit to the candidates in the signal region and sideband is performed. The background fraction is Gaussian-constrained in the fit to $(8.78 \pm 0.05)\%$, as measured in the $m(K^-\pi^+\pi^+)$ fit.

The PDF of σ_t is a histogram template derived directly from the data. In the fit to the D^0 sample, the template is derived assuming that all candidates in the signal region are signal decays. In the fit to the D^+ sample, the template is derived from the candidates in the signal region by subtracting the scaled distribution of the sideband data. The PDF of σ_t for the background is obtained directly from the sideband data.

The lifetime fits are tested on fully simulated data and on sets of data generated by randomly sampling the PDF with parameters fixed to the values found in the fits to the data. All tests yield unbiased results and expected parameter uncertainties, independent of the assumed values of the D^0 and D^+ lifetimes.

The decay-time distributions of the data, with fit projections overlaid, are shown in Fig. 2. The D^0 and D^+ lifetimes are measured to be 410.5 ± 1.1 (stat) \pm

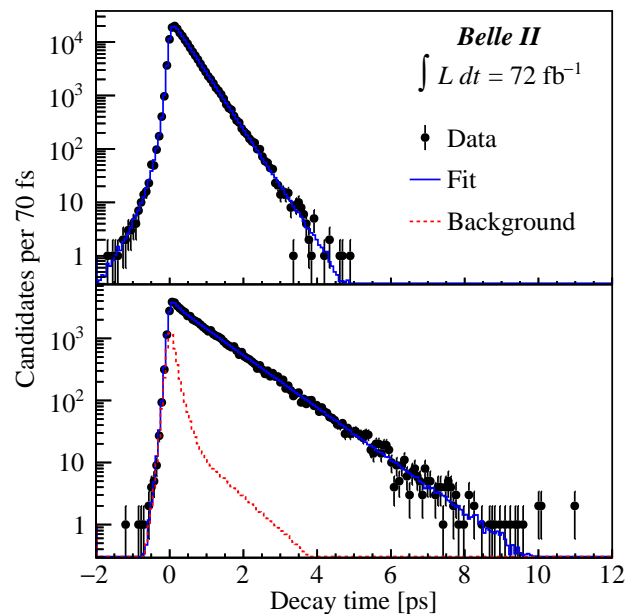


Figure 2: Decay-time distributions of (top) $D^0 \rightarrow K^-\pi^+$ and (bottom) $D^+ \rightarrow K^-\pi^+\pi^+$ candidates in their respective signal regions with fit projections overlaid.

Table I: Systematic uncertainties.

Source	$\tau(D^0)$ [fs]	$\tau(D^+)$ [fs]
Resolution model	0.16	0.39
Backgrounds	0.24	2.52
Detector alignment	0.72	1.70
Momentum scale	0.19	0.48
Total	0.80	3.10

0.8 (syst) fs and 1030.4 ± 4.7 (stat) ± 3.1 (syst) fs, respectively, consistent with their world averages [7]. The systematic uncertainties arise from the sources listed in Table I and described below. The total systematic uncertainty is the sum in quadrature of the individual components.

The decay time and decay-time uncertainty are observed to be correlated in data and simulation reproduces these effects well. The dominant effect is that small σ_t values correspond to larger true decay times (and *vice versa*). These correlations, when neglected in the fits, result in an imperfect description of the t distribution as a function of σ_t . To quantify the impact on the results, our model that neglects the correlations is fit to 1000 samples of signal-only simulated decays, each the same size as the data. The samples are obtained by resampling, with repetition, a set of simulated e^+e^- collisions corresponding to an integrated luminosity of 500 fb^{-1} . Upper bounds of 0.16 fs and 0.39 fs on the average absolute deviations of the measured lifetimes from their true values are derived and assigned as the systematic uncertainty due to the imperfect resolution model for the $D^0 \rightarrow K^-\pi^+$ and

$D^+ \rightarrow K^-\pi^+\pi^+$ cases, respectively. For signal decays, the bias of the decay-time resolution function depends nearly linearly on the candidate mass and may not average out when the mass range is restricted. Varying the boundaries of the signal region shows that such a correlation has a negligible effect upon the measured lifetimes.

The $D^0 \rightarrow K^-\pi^+$ signal region contains per-mille-level background, which is neglected in the lifetime fit and could result in a systematic bias on the measured lifetime. To estimate the size of the bias, we fit our model that neglects the background to 500 resampled sets of simulated e^+e^- collisions, each having the same size and signal-to-background proportion as the data. The measured lifetimes are corrected by subtracting the bias due to the neglected t vs. σ_t correlations. The average absolute difference between the resulting value and the simulated lifetime, 0.24 fs, is assigned as a systematic uncertainty due to the neglected background contamination in the $D^0 \rightarrow K^-\pi^+$ fit.

The background contamination under the $D^+ \rightarrow K^-\pi^+\pi^+$ peak is already accounted for in the fit of the D^+ lifetime using sideband data. In simulation, the sideband (t, σ_t) distribution describes the background (t, σ_t) distribution in the signal region well. The same might not hold in data given that some disagreement is observed between data and simulation in the t distribution of the candidates populating the sideband. We fit to one thousand samples of simulated data obtained by sampling the fit PDF for the signal region and by resampling from the simulated e^+e^- collisions for the sideband. The resulting samples feature sideband data that differ from the background in the signal region with the same level of disagreement as observed between data and simulation. The absolute average difference between the measured and simulated lifetimes, 2.52 fs, is assigned as a systematic uncertainty due to the modeling of the background (t, σ_t) distribution. In the lifetime fit, the fraction of background candidates in the signal region is constrained from the fit to the $m(K^-\pi^+\pi^+)$ distribution. When we change this background fraction to values obtained from fitting to the $m(K^-\pi^+\pi^+)$ distribution with alternative signal and background PDFs, the change in the measured lifetime is negligible.

During data-taking, a periodic calibration determines the alignments and surface deformations of the internal components of the PXD and SVD and the relative alignments of the PXD, SVD, and CDC using e^+e^- -collision, beam-background, and cosmic-ray events [24]. Unaccounted-for misalignment can bias the measurement of the charmed decay lengths and hence their decay times. Two sources of uncertainties associated with the alignment procedure are considered: the statistical precision and a possible systematic bias. Their effects are evaluated using simulated signal-only decays reconstructed with a misaligned detector. For the statistical contribution, we consider configurations derived from comparison

of alignment parameters determined from data acquired on two consecutive days. These configurations have magnitudes of misalignment comparable to the alignment precision as observed in data averaged over a typical alignment period. For the systematic contribution, we consider configurations derived from simulation studies in which coherent global deformations of the vertex detectors (*e.g.*, radial expansion) are introduced [25]. These deformations have magnitudes, determined by the most misaligned sensors, ranging from about 50 μm to 700 μm . The alignment procedure determines the magnitude of these deformations within 4 μm accuracy. We consider configurations in which the CDC is perfectly aligned and configurations in which it is misaligned. Possible effects on the determination of the IR are also introduced by using parameters measured on misaligned samples of simulated $e^+e^- \rightarrow \mu^+\mu^-$ events, to fully mimic the procedure used for real data. For each misalignment configuration, we fit to the reconstructed signal candidates and estimate the lifetime bias. We estimate the systematic uncertainty due to imperfect detector alignment as the sum in quadrature of the largest biases observed in each of the statistical and systematic contributions. The resulting uncertainties are 0.72 fs and 1.70 fs for $D^0 \rightarrow K^-\pi^+$ and $D^+ \rightarrow K^-\pi^+\pi^+$ decays, respectively. The absolute length scale of the vertex detector is determined with a precision significantly better than 0.01% and contributes negligibly to the systematic uncertainty.

The measurement of momenta is calibrated using high-yield charmed-, strange-, and bottom-hadron decays. Uncertainty in the scaling of the momenta results in a systematic uncertainty in the lifetimes of 0.19 fs for D^0 and 0.48 fs for D^+ . Uncertainties in the world averages of the D^0 and D^+ masses [7] contribute negligibly to the systematic uncertainty.

As a cross-check, a statistically independent measurement of the D^0 lifetime is performed using approximately 146×10^3 $D^{*+} \rightarrow D^0(\rightarrow K^-\pi^+\pi^-\pi^+)\pi^+$ decays reconstructed in data with criteria similar to those used for the $D^0 \rightarrow K^-\pi^+$ mode and a signal purity greater than 99%. The resulting lifetime, 408.8 ± 1.2 (stat) fs, agrees with the value determined from the $D^0 \rightarrow K^-\pi^+$ mode.

Finally, the internal consistency of the measurement is tested by repeating the full analysis on various subsets of the data, *i.e.*, running periods and running conditions, charmed-meson momentum and flight direction, and D^{*+} or D^{*-} candidates. We have also studied different selection criteria and sideband definitions. In all cases, the resulting changes in the lifetimes are insignificant and consistent with statistical fluctuations.

In conclusion, the D^0 and D^+ lifetimes are measured using $e^+e^- \rightarrow c\bar{c}$ data collected by Belle II corresponding to an integrated luminosity of 72 fb^{-1} . The results,

$$\tau(D^0) = 410.5 \pm 1.1 \text{ (stat)} \pm 0.8 \text{ (syst)} \text{ fs} \quad \text{and} \quad (1)$$

$$\tau(D^+) = 1030.4 \pm 4.7 \text{ (stat)} \pm 3.1 \text{ (syst)} \text{ fs}, \quad (2)$$

are the world's most precise to date and are consistent with previous measurements [7]. Assuming that all systematic uncertainties are fully correlated between the two measurements, except those due to the background contamination (assumed uncorrelated), the total correlation coefficient is 18%. The ratio of lifetimes is $\tau(D^+)/\tau(D^0) = 2.510 \pm 0.013$ (stat) ± 0.007 (syst). These results demonstrate the vertexing capabilities of the Belle II detector and confirm our understanding of systematic effects that impact future decay-time-dependent analyses of neutral-meson mixing and mixing-induced CP violation.

We thank the SuperKEKB group for the excellent operation of the accelerator; the KEK cryogenics group for the efficient operation of the solenoid; the KEK computer group for on-site computing support; and the raw-data centers at BNL, DESY, GridKa, IN2P3, and INFN for off-site computing support. This work was supported by the following funding sources: Science Committee of the Republic of Armenia Grant No. 20TTCG-1C010; Australian Research Council and research grant Nos. DP180102629, DP170102389, DP170102204, DP150103061, FT130100303, FT130100018, and FT120100745; Austrian Federal Ministry of Education, Science and Research, Austrian Science Fund No. P 31361-N36, and Horizon 2020 ERC Starting Grant no. 947006 ‘‘InterLeptons’’; Natural Sciences and Engineering Research Council of Canada, Compute Canada and CANARIE; Chinese Academy of Sciences and research grant No. QYZDJ-SSW-SLH011, National Natural Science Foundation of China and research grant Nos. 11521505, 11575017, 11675166, 11761141009, 11705209, and 11975076, LiaoNing Revitalization Talents Program under contract No. XLYC1807135, Shanghai Municipal Science and Technology Committee under contract No. 19ZR1403000, Shanghai Pujiang Program under Grant No. 18PJ1401000, and the CAS Center for Excellence in Particle Physics (CCEPP); the Ministry of Education, Youth and Sports of the Czech Republic under Contract No. LTT17020 and Charles University grants SVV 260448 and GAUK 404316; European Research Council, 7th Framework PIEF-GA-2013-622527, Horizon 2020 ERC-Advanced Grants No. 267104 and 884719, Horizon 2020 ERC-Consolidator Grant No. 819127, Horizon 2020 Marie Skłodowska-Curie grant agreement No. 700525 ‘‘NIOBE,’’ and Horizon 2020 Marie Skłodowska-Curie RISE project JENNIFER2 grant agreement No. 822070 (European grants); L’Institut National de Physique Nucléaire et de Physique des Particules (IN2P3) du CNRS (France); BMBF, DFG, HGF, MPG, and AvH Foundation (Germany); Department of Atomic Energy under Project Identification No. RTI 4002 and Department of Science and Technology (India); Israel Science Foundation grant No. 2476/17, United States-Israel Binational Science Foundation grant No. 2016113, and Israel Ministry of Science grant No. 3-16543;

Istituto Nazionale di Fisica Nucleare and the research grants BELLE2; Japan Society for the Promotion of Science, Grant-in-Aid for Scientific Research grant Nos. 16H03968, 16H03993, 16H06492, 16K05323, 17H01133, 17H05405, 18K03621, 18H03710, 18H05226, 19H00682, 26220706, and 26400255, the National Institute of Informatics, and Science Information NETwork 5 (SINET5), and the Ministry of Education, Culture, Sports, Science, and Technology (MEXT) of Japan; National Research Foundation (NRF) of Korea Grant Nos. 2016R1D1A1B-01010135, 2016R1D1A1B02012900, 2018R1A2B3003643, 2018R1A6A1A06024970, 2018R1D1A1B07047294, 2019K1A3A7A09033840, and 2019R111A3A01058933, Radiation Science Research Institute, Foreign Large-size Research Facility Application Supporting project, the Global Science Experimental Data Hub Center of the Korea Institute of Science and Technology Information and KREONET/GLORIAD; Universiti Malaya RU grant, Akademi Sains Malaysia and Ministry of Education Malaysia; Frontiers of Science Program contracts FOINS-296, CB-221329, CB-236394, CB-254409, and CB-180023, and SEP-CINVESTAV research grant 237 (Mexico); the Polish Ministry of Science and Higher Education and the National Science Center; the Ministry of Science and Higher Education of the Russian Federation, Agreement 14.W03.31.0026, and the HSE University Basic Research Program, Moscow; University of Tabuk research grants S-0256-1438 and S-0280-1439 (Saudi Arabia); Slovenian Research Agency and research grant Nos. J1-9124 and P1-0135; Agencia Estatal de Investigacion, Spain grant Nos. FPA2014-55613-P and FPA2017-84445-P, and CIDEAGENT/2018/020 of Generalitat Valenciana; Ministry of Science and Technology and research grant Nos. MOST106-2112-M-002-005-MY3 and MOST107-2119-M-002-035-MY3, and the Ministry of Education (Taiwan); Thailand Center of Excellence in Physics; TUBITAK ULAKBIM (Turkey); Ministry of Education and Science of Ukraine; the US National Science Foundation and research grant Nos. PHY-1807007 and PHY-1913789, and the US Department of Energy and research grant Nos. DE-AC06-76RLO1830, DE-SC0007983, DE-SC0009824, DE-SC0009973, DE-SC0010073, DE-SC0010118, DE-SC0010504, DE-SC0011784, DE-SC0012704, DE-SC0021274; and the Vietnam Academy of Science and Technology (VAST) under grant DL0000.05/21-23.

-
- [1] M. Neubert, *Adv. Ser. Direct. High Energy Phys.* **15**, 239 (1998), arXiv:hep-ph/9702375 .
 - [2] N. Uraltsev, in *At the frontier of Particle Physics*, edited by M. Shifman and B. Ioffe (2001) arXiv:hep-ph/0010328 .
 - [3] A. Lenz and T. Rauh, *Phys. Rev. D* **88**, 034004 (2013), arXiv:1305.3588 [hep-ph] .

- [4] A. Lenz, *Int. J. Mod. Phys. A* **30**, 1543005 (2015), arXiv:1405.3601 [hep-ph] .
- [5] M. Kirk, A. Lenz, and T. Rauh, *JHEP* **12**, 068 (2017), [Erratum: *JHEP* **06** (2020) 162], arXiv:1711.02100 [hep-ph] .
- [6] H.-Y. Cheng, *JHEP* **11**, 014 (2018), arXiv:1807.00916 [hep-ph] .
- [7] P. A. Zyla *et al.* (Particle Data Group), *PTEP* **2020**, 083C01 (2020).
- [8] J. M. Link *et al.* (FOCUS collaboration), *Phys. Lett. B* **537**, 192 (2002), arXiv:hep-ex/0203037 .
- [9] R. Aaij *et al.* (LHCb collaboration), *Phys. Rev. Lett.* **119**, 101801 (2017), arXiv:1705.03475 [hep-ex] .
- [10] R. Aaij *et al.* (LHCb collaboration), *Phys. Rev. Lett.* **121**, 092003 (2018), arXiv:1807.02024 [hep-ex] .
- [11] R. Aaij *et al.* (LHCb collaboration), *Phys. Rev. Lett.* **121**, 052002 (2018), arXiv:1806.02744 [hep-ex] .
- [12] R. Aaij *et al.* (LHCb collaboration), *Phys. Rev. D* **100**, 032001 (2019), arXiv:1906.08350 [hep-ex] .
- [13] T. Abe (Belle II collaboration), (2010), arXiv:1011.0352 [physics.ins-det] .
- [14] K. Akai, K. Furukawa, and H. Koiso, *Nucl. Instrum. Meth.* **A907**, 188 (2018), arXiv:1809.01958 [physics.acc-ph] .
- [15] A. J. Bevan *et al.*, *Eur. Phys. J.* **C74**, 3026 (2014), arXiv:1406.6311 [hep-ex] .
- [16] S. Jadach, B. F. L. Ward, and Z. Was, *Comput. Phys. Commun.* **130**, 260 (2000), arXiv:hep-ph/9912214 [hep-ph] .
- [17] T. Sjöstrand, S. Ask, J. R. Christiansen, R. Corke, N. Desai, P. Ilten, S. Mrenna, S. Prestel, C. O. Rasmussen, and P. Z. Skands, *Comput. Phys. Commun.* **191**, 159 (2015), arXiv:1410.3012 [hep-ph] .
- [18] D. J. Lange, *Proceedings, 7th International Conference on B physics at hadron machines (BEAUTY 2000): Maagan, Israel, September 13-18, 2000*, *Nucl. Instrum. Meth.* **A462**, 152 (2001).
- [19] S. Agostinelli *et al.* (GEANT4 collaboration), *Nucl. Instrum. Meth.* **A506**, 250 (2003).
- [20] T. Kuhr, C. Pulvermacher, M. Ritter, T. Hauth, and N. Braun (Belle-II Framework Software Group), *Comput. Softw. Big Sci.* **3**, 1 (2019), arXiv:1809.04299 [physics.comp-ph] .
- [21] J.-F. Krohn *et al.* (Belle-II analysis software group), *Nucl. Instrum. Meth.* **A976**, 164269 (2020), arXiv:1901.11198 [hep-ex] .
- [22] T. Skwarnicki, *A study of the radiative cascade transitions between the Upsilon-prime and Upsilon resonances*, Ph.D. thesis, Institute of Nuclear Physics, Krakow (1986), DESY-F31-86-02.
- [23] N. L. Johnson, *Biometrika* **36**, 149 (1949).
- [24] T. Bilka *et al.*, *EPJ Web Conf.* **245**, 02023 (2020).
- [25] D. Brown, A. Gritsan, Z. Guo, and D. Roberts, *Nucl. Instrum. Meth.* **A603**, 467 (2009).